Bulletin of Electrical Engineering and Informatics
Vol. 15, No. 4, August 2026, pp. 3598~3609
ISSN: 2302-9285, DOI: 10.11591/eei.v15i4.10704

A reconfigurable 38/60 GHz array antenna for 5G applications

Ahmed El Ghandour[1], Mohamed Nabil Srifi[1], Younes Karfa Bekali[2], Mourad El Habchi[3]
[1]ASE Laboratory, National School of Applied Sciences (ENSA), Ibn Tofail University, Kenitra, Morocco
[2]LRIT Laboratory, Faculty of Sciences, Mohammed V University, Rabat, Morocco
[3]LTI Laboratory, Department of Physics, Faculty of Sciences, Hassan II University, Casablanca, Morocco

Article Info

Article history:

Received May 17, 2025
Revised May 7, 2026
Accepted Jul 9, 2026

Keywords:

Broadband antenna array
Fifth generation
High gain
Mm-wave
Reconfigurable frequency array antenna

ABSTRACT

The aim of this paper is to propose a 4-element frequency-reconfigurable antenna array operating at 38 GHz and 60 GHz for fifth generation (5G) applications. The proposed structure integrates three radiating elements into a single patch, enabling compactness and improved performance. The antenna achieves dual-band reconfigurability with gains of 12.65 dBi and 15.54 dBi at 38 GHz and 60 GHz, respectively. Excellent impedance matching is obtained, with S11 values of -51.82 dB and -33.79 dB at the two resonant frequencies. Frequency switching is controlled through positive–intrinsic–negative (PIN) diodes embedded in the ground-plane slot. The antenna design was modeled and validated through full-wave simulations using computer simulation technology (CST) studio suite.

Corresponding Author:

Ahmed El Ghandour
ASE Laboratory, National School of Applied Sciences (ENSA), Ibn Tofail University
Kenitra, Morocco
Email: ahmed.elghandour@uit.ac.ma

1. INTRODUCTION

The millimeter-wave (mmWave) spectrum, spanning 30 GHz to 300 GHz, is the cornerstone of modern wireless communications [1], providing the necessary bandwidth for the multi-gigabit-per-second data rates and low latency required by fifth generation (5G) mobile systems [1], [2]. Antenna design efforts are primarily focused on the 28 GHz, 38 GHz, and 60 GHz bands [1], [3] where severe propagation loss and multipath interference necessitate the development of high-gain, high-efficiency antenna arrays [4]. To address signal degradation and absorption, especially within the license-exempt 60 GHz band [4], circularly polarized (CP) antennas are widely favored [4]. Specific 60 GHz design examples include high-gain monopole antenna arrays [5], multiple-input multiple-output (MIMO) microstrip antennas [6] including an ultra-wide patch arrays for remote vital sign monitoring [7], and specialized arrays for 3D antenna-in-package (AiP) applications [8]. Additional 60 GHz solutions feature designs utilizing gap waveguide technology and glide symmetries for double slot arrays [9], compact series-fed patch arrays for automotive radar systems like rear occupant alert (ROA), which must overcome the inherently limited bandwidth of microstrip patches [10], phased arrays with unique key-shaped elements for efficient beam steering [11], and miniaturized comb-shaped microstrip antennas for high gain [12].

Furthermore, to ensure 5G device versatility, multiband antennas are critical, with numerous designs proposed for the 28/38 GHz bands, such as compact dual-band MIMO systems [3], flexible dual-band 4×4 MIMO for wearable applications [13], quad-port cross-shaped antennas with improved isolation [14], high-gain single-element microstrip bi-band antennas as a less complex alternative to arrays [15], and other dual-band models employing internal stubs and slot perturbations [16] or stub resonators [17]. Finally, broader frequency coverage is achieved with dual-band (38/60 GHz) patch antennas for mobile handsets [1], tri-band antennas covering 5G Ka- and V-band spectras (28 GHz and 44 GHz) [18], and wide-spectrum arrays designed to operate across 28/38/60/70/80 GHz for mobile applications [19]. Many current studies lack the flexibility offered by dynamic operation. To address this limitation, we introduce a reconfigurability function in our proposed design, allowing for effective control and switching between the critical target 38 GHz (5G Ka-band) and 60 GHz (V-band) frequency bands.

The aim of this article is to propose a reconfigurable 38/60 GHz array antenna for 5G applications. We started by designing a single patch antenna that incorporates three radiator elements to enhance gain and other performance parameters. Subsequently, we integrated a positive–intrinsic–negative (PIN) diode for reconfigurability. The final proposal involves an array of four antennas, utilizing PIN diodes in the ground plane for switching capabilities. Computer simulation technology (CST) studio suite was used to perform all antenna simulations. The comprehensive plan for presenting the analysis begins with the introduction and antenna design and geometry, followed by the results and discussion which details the reflection coefficients and voltage standing wave ratio (VSWR) of the evolution stages, gain, radiation patterns, reconfigurability, and the performance of the 4-element array. The paper concludes with related works and the final conclusion.

2. ANTENNA DESIGN AND GEOMET

The proposed antenna configuration, illustrated in Figure 1, is designed on a Rogers RT/Duroid 5880 substrate. This is a low-loss dielectric material with a thickness of h=0.254 mm, a relative permittivity of εr=2.2, and a loss tangent of 0.0009. The antenna's overall dimensions are determined by the size of the substrate itself. The top surface of the antenna, as shown in Figure 1(a), features a single copper radiator fed by a microstrip line. The feed line consists of a main section (Wf1×Lf1) that transitions to a wider matching section (Wf2×Lf2) before connecting to the main radiating element. The radiator itself is a composite structure comprised of three interconnected rectangular sections: a central patch (Wp×Lp), a second patch (Wp1×Lp1), and a large top radiator (Wp2×Lp2). The bottom surface of the substrate, depicted in Figure 1(b), includes a partial ground plane with a centrally etched rectangular slot.

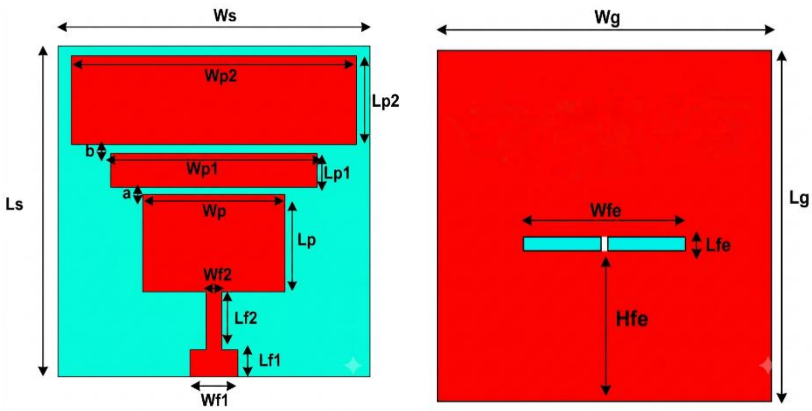

(a) (b)

Figure 1. Geometrical configuration of the proposed antenna; (a) top view and (b) bottom view

This slot has dimensions of Wfe×Lfe and is positioned at a distance of Hfe from the bottom edge of the ground plane. The specific parameters for this antenna, detailed in Table 1, were calculated using the equations referenced in [20], [21]. The design was simulated using CST software. The step-by-step evolution of this antenna is shown in Figures 2(a) to (d). The next section of the paper will discuss the simulation results and analyze the impact of each design step on the antenna's performance.

Table 1. Design parameters of the antenna

Parameters	Lg	Wg	Ls	Ws	h	t	Lp	Wp	Lp1	Wp1	Wfe
Values (mm)	5.5	8	5.5	8	0.254	0.035	1.45	2.2	0.6	3.2	2.2
Parameters	Lp2	Wp2	Lf1	Wf1	Lf2	Wf2	a	b	Hfe	Lfe	
Values (mm)	1.3	4.4	0.84	0.26	0.84	0.78	0.1	0.1	2.56	0.36	

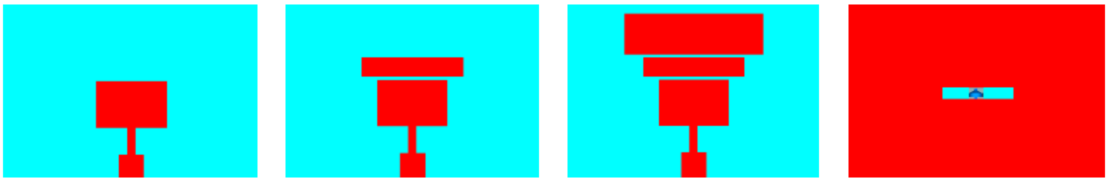

(a) (b) (c) (d)

Figure 2. Evolution stages of the proposed antenna; (a) step 1, (b) step 2, (c) step 3, and (d) back view

3. RESULTS AND DISCUSSION

In this section, we explore the patch antenna’s performance, and we present and discuss the related numerical results.

3.1. Reflection coefficients and voltage standing wave ratio of evolution stages

The results presented in Figure 3 illustrate the antenna’s performance evolution through three stages, evaluated by its return loss (S11) and VSWR across the 50–70 GHz frequency range. As shown in Figure 3(a), the S11 plot indicates that the initial antenna design (without directors) resonates at 60.14 GHz with a return loss of −33.187 dB. Introducing the first director shifts the resonant frequency to 57.7 GHz and significantly enhances impedance matching, achieving an S11 of −55.013 dB, the best performance among the three configurations. Adding a second director slightly increases the resonant frequency to 58.94 GHz, while the S11 value decreases to -29.872 dB. All three resonant frequencies (57.7 GHz, 58.94 GHz, and 60.14 GHz) lie within the mmWave band, making the proposed design suitable for 5G and future wireless communication application. The results of VSWR plot as shown in Figure 3(b) confirms the excellent impedance matching observed in the S11 analysis. For all three configurations, the VSWR is well under the acceptable threshold of 2. The lowest VSWR of 1.0036 corresponds to the one-director configuration (57.7 GHz), which is nearly ideal (VSWR=1), reinforcing its superior performance in terms of reflected power. The values of 1.0448 (without directors) and 1.0663 (with two directors) also represent very good matching. The consistently low VSWR across all steps indicates that the antenna works under good operating conditions throughout its evolution.

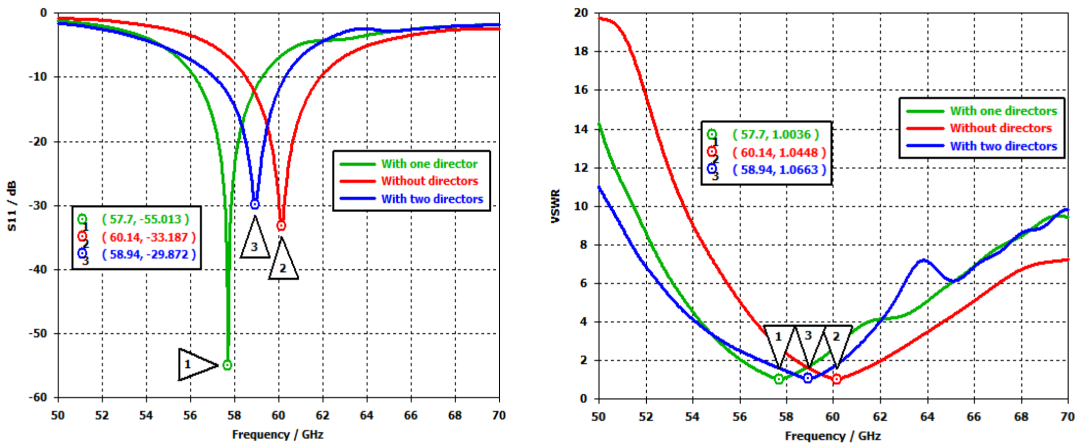

(a) (b)

Figure 3. Reflection coefficients; (a) VSWR and (b) of evolution stages

3.2. Gain performance

The gain of a patch antenna, which reflects its directivity and radiation efficiency, defines its ability to concentrate energy in a specific direction. Figure 4 presents the simulated gain performance across the different evolution stages of the proposed antenna. As shown in Figure 4(a), the reference antenna (without directors) achieves a gain of 8.5 dBi. Introducing the first director slightly increases the gain to 8.77 dBi, as illustrated in Figure 4(b). With the addition of a second director, the gain further improves to 10.07 dBi, as shown in Figure 4(c). This progressive enhancement confirms the effectiveness of the director elements in improving antenna gain and directivity.

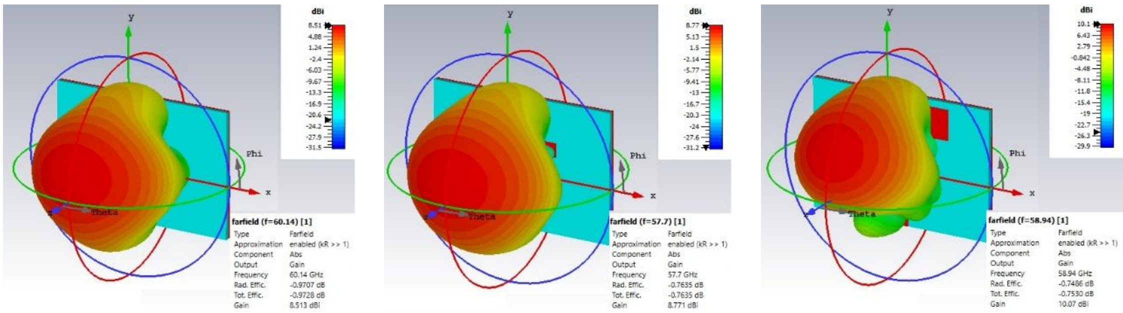

(a) (b) (c)

Figure 4. The simulated gain for different evolution stages; (a) step 1, (b) step 2, and (c) step 3

3.3. Radiation patterns

Figure 5 presents the 2D radiation patterns of the antenna across the different design stages. In step 1 at 60.14 GHz, shown in Figure 5(a), the antenna exhibits a broad and symmetrical pattern with moderate gain and visible back lobes. The introduction of the first director in step 2 at 57.7 GHz, as illustrated in Figure 5(b), focuses the radiation, improving gain and reducing back radiation. With the addition of two directors in step 3 at 58.94 GHz, depicted in Figure 5(c), the E-plane displays a highly directional main lobe and significantly enhanced gain, while the H-plane becomes slightly asymmetric. Overall, the results confirm that adding directors effectively improves antenna directivity and beam shaping.

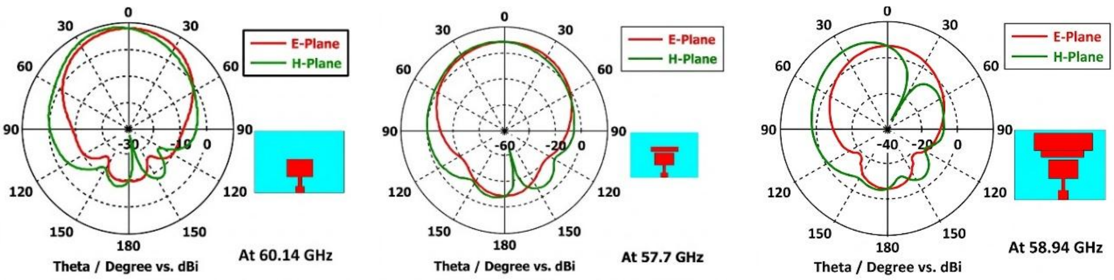

(a) (b) (c)

Figure 5. The corresponding 2D radiation patterns for different stages; (a) step 1, (b) step 2, and (c) step 3

3.4. Effect of varying the parameters of a single antenna

Needless to say, through this parametric study, the dimensions and the position of the director elements and the slot incorporated in the ground plane have a relative effect on the resonance frequency, return loss, and produce also a noticeable change in the antenna gain. From the outcomes of this study, we tried to rely on the configuration that allows us to maintain the resonance frequency around the desired band while achieving the highest gain and the best reflection coefficient. This is the configuration that was initially approved in Table 1.

3.4.1. Reflection coefficient

Figure 6 illustrates the parametric study of the antenna's reflection coefficient (S_{11}) under various geometrical variations. Figure 6(a) illustrates that decreasing the parameter "a" of the first director element (i.e., increasing its spacing relative to the radiating patch) has two primary effects. First, it causes a decrease in the resonant frequency (shifting from ~58.4 GHz to ~57.4 GHz). Second, it leads to a degradation of the reflection coefficient (S_{11}), as the minimum value increases (worsening from -37 dB to -33 dB). Generally, increased spacing modifies the capacitive coupling effect between the radiating element and the director, adjusting the total reactance perceived by the antenna. This, in turn, shifts the resonant frequency and affects the quality of the impedance matching.

Similarly, Figure 6(b) shows the impact of varying the parameter "b" of the second director. Increasing "b" (the spacing) also leads to a decrease in the resonant frequency (shifting from ~59.2 GHz to ~58.8 GHz). Furthermore, this increase worsens the impedance match, as indicated by the increase in the minimum S_{11} (from -35 dB to -30 dB). These observations confirm that the spacing between director elements is crucial for controlling the operational frequency and optimizing the antenna's match.

Figure 6(c) illustrates the significant impact of the second director element's dimensions, L_{p1} and W_{p1}, on the antenna's performance. This element acts as the secondary tuning element for both frequency and impedance matching. Varying L_{p1} from 0.2 to 0.6 mm causes a substantial downward shift in the resonant frequency, moving the minimum S_{11} from approximately 59.5 GHz down to 57.8 GHz. Furthermore, optimizing these dimensions leads to an excellent impedance match, with the combination of $L_{p1} = 0.6$ mm and $W_{p1} = 3.2$ mm achieving the deepest return loss of around -55 dB. This depth indicates that the $p1$ element is crucial for achieving high-quality energy transfer and low reflection at the desired operating frequency.

Figure 6(d) shows the effect of varying the third director element's dimensions, L_{p2} and W_{p2}. In contrast to $p1$, this element functions as a tertiary tuning element, offering only minor adjustments to the overall performance. The best return loss achieved by optimizing $p2$ parameters is significantly poorer, peaking at only about -20 dB (e.g., $L_{p2} = 1.1$ mm and $W_{p2} = 4.4$ mm). Moreover, changing L_{p2} from 1.1 to 1.3 mm results in a very slight upward frequency shift (from 58 GHz to 58.4 GHz), demonstrating a much weaker influence on the resonance compared to $p1$. This suggests the $p2$ element is likely used for fine-tuning the operating frequency or perhaps optimizing a secondary characteristic like the antenna's gain or radiation pattern, rather than for primary impedance matching.

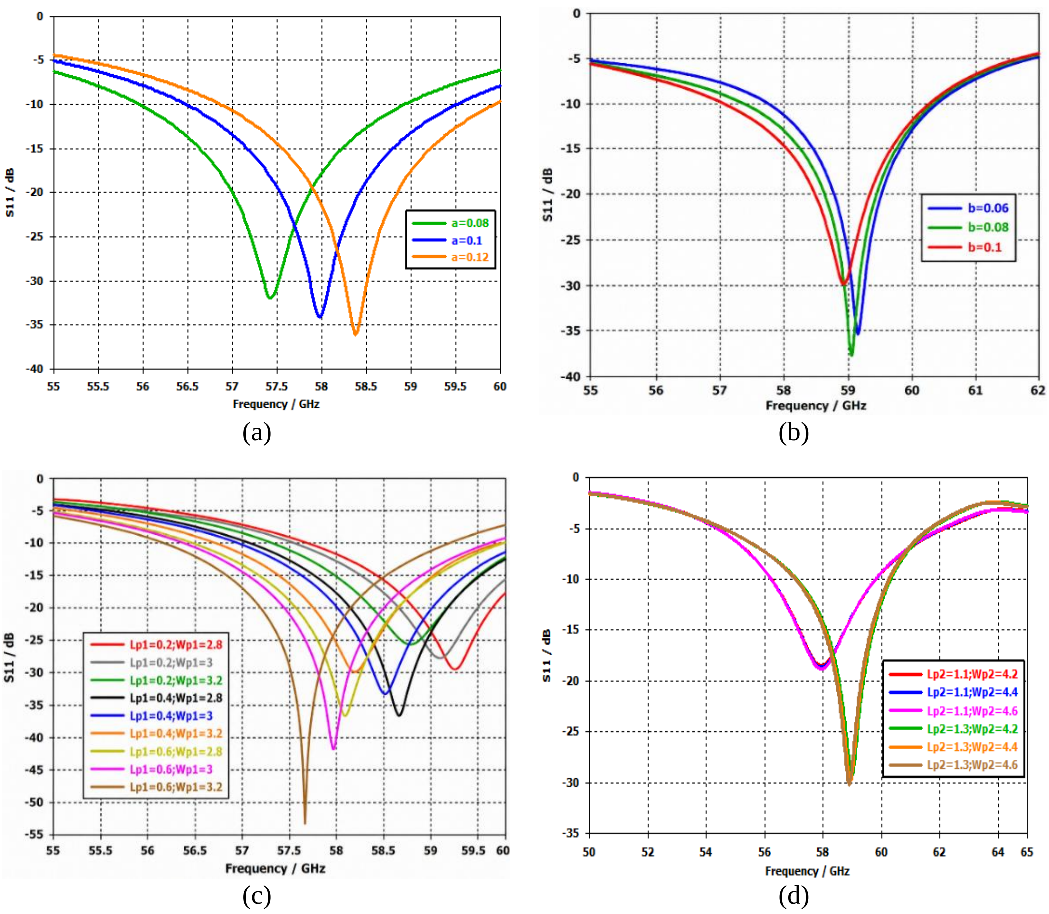

Figure 6. The effect of varying the position and dimensions of the director elements on return loss; (a) spacing parameter a, (b) spacing parameter b, (c) second director dimensions (L_{p1}, W_{p1}), and (d) third director dimensions (L_{p2}, W_{p2})

Figure 7 illustrates the parametric study of the slot's position and dimensions on the antenna's return loss. As shown in Figure 7(a), the vertical position of the slot, H_{fe}, is a critical parameter for both frequency control and impedance matching. As the position of the slot is increased (moving from $H_{fe} = 2.5$ mm to $H_{fe} = 2.6$ mm), the resonant frequency shifts to a higher value (from ~37.8 GHz to ~38.2 GHz). Simultaneously, the impedance matching significantly improves, with the S_{11} minimum deepening from -20 dB to an excellent -32 dB. This confirms that the slot acts as a coupling mechanism between the microstrip feed line and the patch, and its position is paramount in tuning the resonance to the desired band while optimizing power transfer.

Figure 7(b) further shows that the slot dimensions (L_{fe} and W_{fe}) are the dominant factor for determining the exact resonant frequency. Increasing the slot length (L_{fe}) causes a substantial shift to a lower frequency, which is characteristic of a radiating element as its effective electrical length increases. Furthermore, these dimensions are crucial for the coupling strength, as indicated by the wide variation in impedance match quality (from -15 dB to -39 dB). The best performance, achieving $S_{11} \approx -39$ dB at 36.6 GHz, is obtained for the largest tested length ($L_{fe} = 0.42$ mm) and smaller width ($W_{fe} = 2.2$ mm), proving that precise control over the slot's geometry is necessary to tune the antenna for optimal operation.

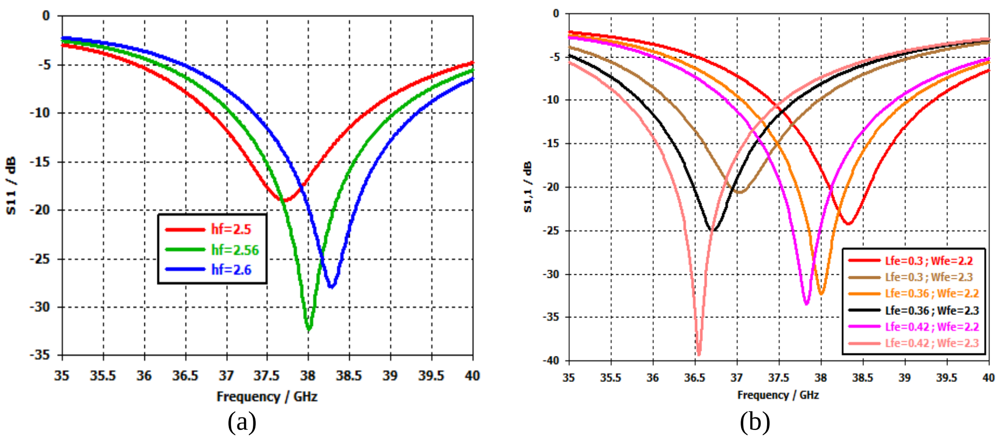

Figure 7. The effect of varying the position and dimensions of the slot on return loss in; (a) slot vertical position H_{fe} and (b) slot dimensions L_{fe} and W_{fe}

3.4.2. Parametric analysis of gain

Figure 8 presents the parametric analysis of the antenna's gain under various position and dimensional variations of the director elements. Figure 8(a) shows the gain as a function of the parameter a. The parameter a exhibits an inverse relationship with the gain. As the frequency increases (from 55 GHz to 60 GHz), the gain generally increases for all values of a. However, at any fixed frequency, a decrease in a (from 0.12 to 0.08 mm) leads to a higher gain. The highest gain is achieved with the smallest value, $a = 0.08$ mm. Conversely, the parameter b exhibits a direct relationship with the gain, as shown in Figure 8(b). Across the frequency band (58 GHz to 60 GHz), a higher value of b (from 0.06 to 0.1 mm) results in a higher gain, reaching the highest overall gain with $b = 0.1$ mm. Therefore, to maximize the gain across these two parameter variations, one should select the smallest possible value for a and the largest possible value for b.

As illustrated in Figures 8(c) and (d), increasing the size of the director elements while reducing the spacing between the first director and the patch antenna (a) leads to a significant improvement in gain. In Figure 8(c), increasing a (from 0.08 to 0.12 mm) while fixing the dimensions of the first director element results in a decrease in gain (from 8.74 dBi to 8.7 dBi). Conversely, increasing the dimensions of the first director element (from $L_{p1} = 0.2$ mm, $W_{p1} = 2.8$ mm to $L_{p1} = 0.6$ mm, $W_{p1} = 3.2$ mm) while fixing $a = 0.1$ mm increases the gain from 8.42 dBi to 8.77 dBi. As shown in Figure 8(d) for a fixed $b = 0.1$ mm, increasing the dimensions of the second director element (from $L_{p2} = 1.1$ mm, $W_{p2} = 4.2$ mm to $L_{p2} = 1.3$ mm, $W_{p2} = 4.4$ mm) increases the gain from 9.62 dBi to 10.07 dBi. The results demonstrate a clear trend: larger director dimensions enhance wave-guiding effects, concentrating radiation in the desired direction, while minimizing the director-patch distance strengthens mutual coupling, further optimizing directivity.

Figure 9 illustrates the parametric study of the slot position and dimensions on the antenna gain. Figure 9(a) demonstrates the effect of the slot position H_{fe} on gain across the 35 GHz to 40 GHz band, revealing a frequency-dependent optimization. While the general trend suggests that increasing H_{fe} towards 2.6 mm is beneficial for maximizing gain at the band edges—particularly at 40 GHz where $H_{fe} = 2.6$ mm achieves ≈ 5.42 dBi—the performance is non-linear elsewhere. At the specific frequency of 38 GHz, the highest gain of approximately 5.23 dBi is achieved by the maximum value, $H_{fe} = 2.6$ mm, indicating that optimal tuning of this parameter is necessary for peak performance within the operational bandwidth.

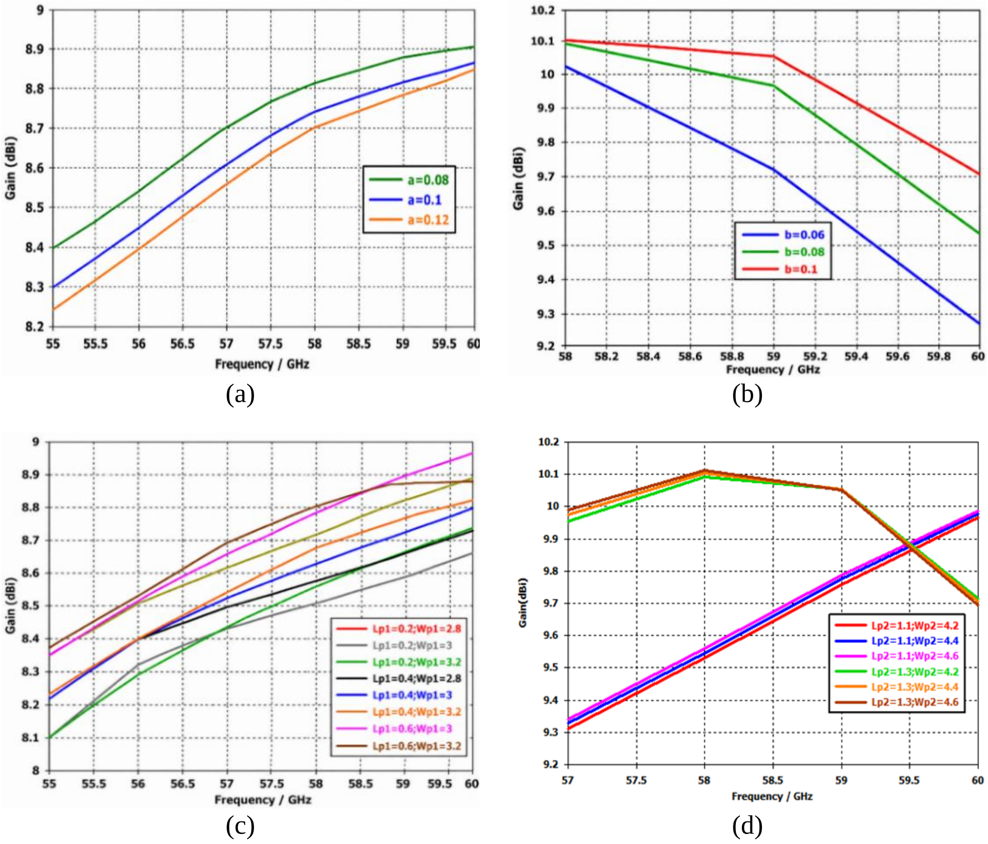

Figure 8. The effect of varying the position and dimensions of the director elements on gain in; (a) position parameter a, (b) position parameter b, (c) dimensions L_{p1} and W_{p1} of the second director, and (d) dimensions L_{p2} and W_{p2} of the third director

Focusing on the operating frequency of 38 GHz, Figure 9(b) evaluates the impact of slot dimension combinations (L_{fe} and W_{fe}). The highest gain at 38 GHz is achieved by two combinations: $L_{fe} = 0.3$ mm, $W_{fe} = 2.2$ mm (achieving ≈ 5.25 dBi) and $L_{fe} = 0.36$ mm, $W_{fe} = 2.2$ mm (achieving ≈ 5.18 dBi). This indicates that a wider slot width ($W_{fe} = 2.2$ mm) is favorable for maximizing gain at this frequency, regardless of whether the slot length is 0.3 mm or 0.36 mm. Conversely, the lowest gain at 38 GHz is produced by $L_{fe} = 0.42$ mm and $W_{fe} = 2.3$ mm, resulting in approximately 4.86 dBi. This performance drop suggests that this specific combination creates a detrimental impedance mismatch or radiation pattern null at 38 GHz, making it the poorest choice for the 38 GHz band.

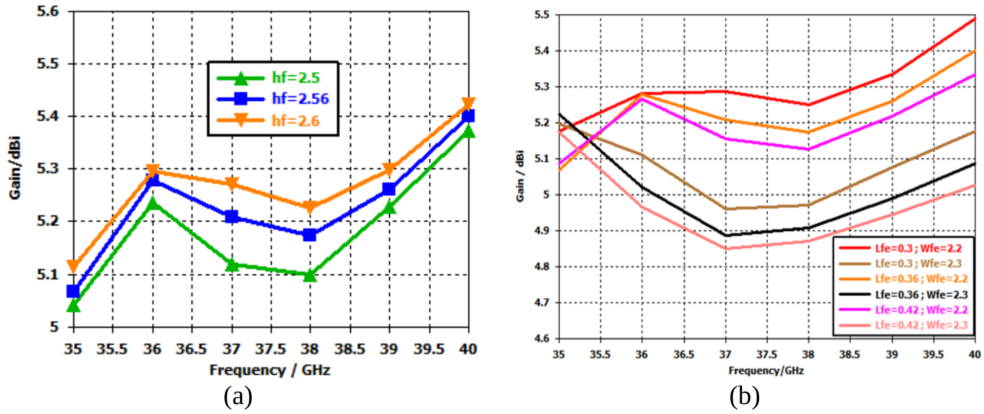

Figure 9. The effect of varying the position and dimensions of the slot on gain in; (a) slot vertical position H_{fe} across 35–40 GHz and (b) slot dimension combinations L_{fe} and W_{fe} at 38 GHz

3.5. Reconfigurability function

Figure 10 illustrates the reconfigurability mechanism of the proposed antenna, including the integration of the PIN diode within the ground plane and its electrical modeling. As shown in Figure 10(a), antenna reconfigurability is realized using a PIN diode embedded in the ground-plane slot to switch operation between the 38 GHz and 60 GHz bands. The equivalent circuit model of the PIN diode [22] is presented in Figure 10(b). The diode parameters for each state are: ON state (L = 0.7 nH and R_s = 5 Ω) and OFF state (L = 0.7 nH, R_s = 5 kΩ, and C_T = 0.2 pF) [23].

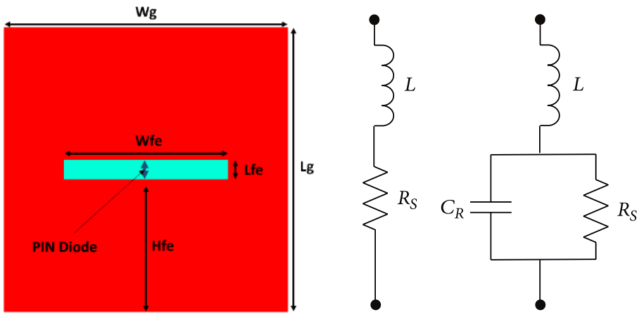

(a) (b)

Figure 10. Reconfigurability mechanism of the proposed antenna showing; (a) PIN diode integrated in the ground plane slot and (b) its equivalent circuit model

When the PIN diode is ON, it acts as a short circuit, effectively closing the slot. This state activates the 60 GHz band, resulting in a strong resonance near 59 GHz (an S_{11} of -23 dB) while suppressing the 38 GHz resonance. Conversely, when the PIN diode is OFF, it acts as a capacitor, leaving the slot open. This state activates the 38 GHz band, producing a deep resonance near 38.5 GHz (S_{11} below -30 dB) while suppressing the 60 GHz resonance. The reference cases confirm this mechanism: the "Slotted without PIN diode" case is identical to the OFF state, enabling the 38 GHz band, and the "Without slot" case eliminates the 38 GHz resonance entirely, leaving only the 59 GHz resonance. Thus, the PIN diode successfully provides binary frequency switching between the 38 GHz and 60 GHz operating bands, as confirmed by the reflection coefficient comparison shown in Figure 11.

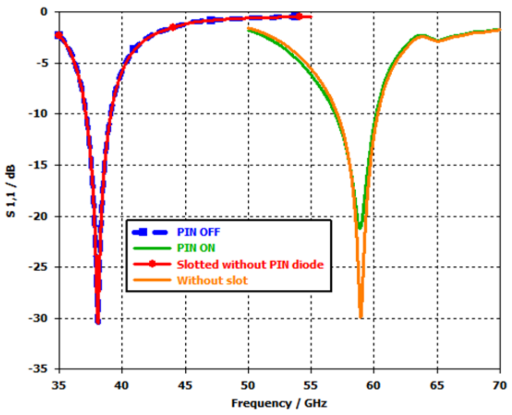

Figure 11. Comparison of the antenna reflection coefficient in different cases

3.6. 4-element array

Despite the many advantages offered by the 60 GHz band, the biggest obstacle remains its free-space path loss and particularly high oxygen absorption, which we aim to overcome by increasing the antenna gain through the design of antenna arrays. We have employed mitered bends to compensate for the excess capacitance and prevent reflections, thereby restoring the line's original characteristic impedance, as transmission line discontinuities such as 90° bends in a T-junction introduce parasitic reactance [24]. Figure 12 presents the layout and detailed dimensions of the proposed 4-element antenna array. As shown in Figure 12(a), the complete array configuration incorporates the optimized power division feeding network with mitered bends and four radiating elements. Figure 12(b) provides the specific geometrical dimensions of the feeding network structure (detailed in Table 2), while keeping the individual patch dimensions fixed as previously defined in Table 1.

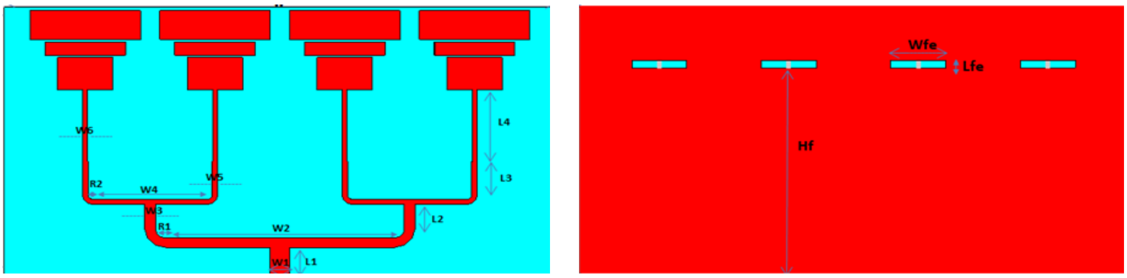

(a) (b)

Figure 12. The 4-elements array; (a) top view and (b) bottom view

Table 2. The array design parameters (all values are in millimeters)

Parameters	W1	L1	W2	L2	W3	L3	W4	L4	W5
Values (mm)	0.78	1.26	9.14	1.1	0.42	1.5	4.55	3.2	0.23
Parameters	W6	Wfe	Lfe	W	L	R1	R2	Hf	
Values (mm)	0.18	2.2	0.36	22	12	0.4	0.2	9.13	

As depicted in Figure 13, the simulated results show the ability of the 4-elements array to change its frequencies by changing the PIN diodes modes. The obtained gain results are very promising, and the desired results are achieved. In this regard, and for the 4-element array, we note that a high gain of 12.65 dBi was obtained at 38.75 GHz frequency (38 band=OFF state), while for the 60 band (ON state), a gain of 15.64 dBi was obtained at 60 GHz. Table 3 summarizes all the results obtained for the antenna array in both operating modes (ON and OFF).

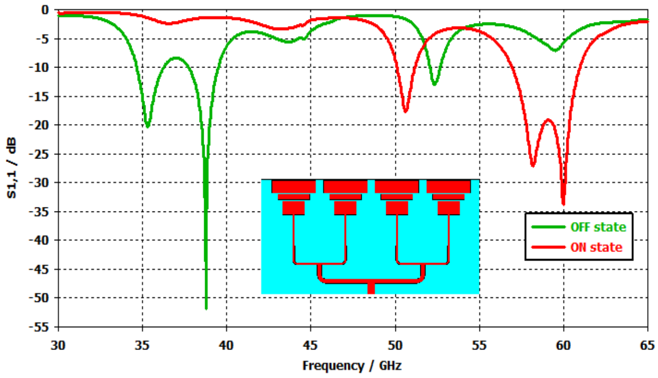

Figure 13. Reflection coefficient of different states of the 4-elements array

Table 3. The array performances and their corresponding frequencies

Array	4-elements					
State		Off			On	
Frequency (GHz)	35.28	38.75	52.36	50.61	58.17	60
S11 (dB)	-20.22	-51.82	-12.92	-17.74	-27.05	-33.79
Gain (dBi)	11.93	12.65	11.64	14.19	15.64	15.54

4. RELATED WORKS

The elementary antenna and its resulting array detailed comparative analysis with similar types reported in the literature is presented in Table 4. They present strong contenders for 5G applications due to their compact size, high gain, and reconfigurability between the 38 GHz and 60 GHz bands. These frequencies are highly promising for 5G, offering wide bandwidth and high-speed connectivity. The structures achieve competitive performance in both bands, making it adaptable for diverse 5G applications.

Table 4. Comparison of all antennas at the 38/60 GHz bands

Ref.	Antenna type/description	Operating frequency (GHz)	Total size	S11 (dB)	B.W. (|S11| ≤−10 dB) (GHz)	Gain (dBi)
[4]	4×4 CP dual-coil array (60 GHz)	54.6-67.3	5.46×5.48×0.51 λ_0^3	≤−10	12.7 (20.8%)	19.3
[5]	2-element monopole array (60 GHz) avec DGS	57.2-63.8	20.64×20 mm^2	≤−10	6.6	11.6
[7]	Ultra-wide patch array (RVSM/doppler radar)	57.24-65.88	N/A	N/A	8.64	N/A
[8]	1×4 patch array pour 3D AiP	58.46-62.14	12.8×10.87×0.597 mm^3	N/A	3.68	10.51
[9]	4×4 double slot array (GW/glide)	37.20-41.58	N/A	≤−10	4.38 (11.4%)	18.75
[10]	3×1 series-fed array (ROA/automobile)	60.95-66.73	1.41×7.04×0.125 mm^3	≤−10	5.78	10.24
[25]	8-element array+FSS (5G multi-band)	20-65 (Global)	1755 (65×27)	≤−10	45	15
[26]	Planar patch array pour 60 GHz radars	60	N/A	≤−10	4.32 (7.2%)	12
[27]	32-element dual-band IFA (28/38 GHz)	27.9-28.8/ 37.9-38.9	64×123×2 mm^3	≤−10	0.89/0.99	16.52
This work	4-elements array	38/60	22×12×0.254 mm^3	≤−10	1.8/4.02	12.65/15.64

5. CONCLUSION

The main purpose of this work was to design a compact, low-cost, reconfigurable array antenna for the 38 GHz and 60 GHz bands, featuring a small size, minimal reflection coefficient, and high gain, making it a promising candidate for 5G mmWave applications. In future work, we aim to extend the design to an 8-element array to achieve higher gain. Additionally, we plan to develop a reconfigurable beam-steering array while preserving the advantages demonstrated in this study. The future work will also include fabrication, measurement of the proposed antenna, and exploration of techniques such as metamaterials to further enhance its performance.

FUNDING INFORMATION

This work was supported by the Center for Scientific Research Support, Presidency of Ibn Tofail University, Kenitra, Morocco.

AUTHOR CONTRIBUTIONS STATEMENT

This journal uses the Contributor Roles Taxonomy (CRediT) to recognize individual author contributions, reduce authorship disputes, and facilitate collaboration.

Name of Author	C	M	So	Va	Fo	I	R	D	O	E	Vi	Su	P	Fu
Ahmed El Ghandour	✓	✓	✓	✓	✓	✓	✓	✓	✓	✓		✓	✓	
Mohamed Nabil Srifi	✓	✓		✓	✓					✓		✓	✓	
Younes Karfa Bekali		✓			✓		✓			✓	✓			
Mourad El Habchi		✓			✓	✓	✓			✓	✓			✓

C : **C**onceptualization
M : **M**ethodology
So : **So**ftware
Va : **Va**lidation
Fo : **Fo**rmal analysis
I : **I**nvestigation
R : **R**esources
D : **D**ata Curation
O : Writing - **O**riginal Draft
E : Writing - Review & **E**diting
Vi : **Vi**sualization
Su : **Su**pervision
P : **P**roject administration
Fu : **Fu**nding acquisition

CONFLICT OF INTEREST STATEMENT

Authors state no conflict of interest

DATA AVAILABILITY

The dataset on which the results of this study are based is publicly available in Tables 1 and 2. The data includes the parameter values used to obtain the results from the CST. Researchers can access the dataset listed in Tables 1 and 2 and use it for further studies.

REFERENCES

[1] M. H. Sharaf, A. I. Zaki, R. K. Hamad, and M. M. M. Omar, “A Novel Dual-Band (38/60 GHz) Patch Antenna for 5G Mobile Handsets,” *Sensors*, vol. 20, no. 9, pp. 1-19, Apr. 2020, doi: 10.3390/s20092541.

[2] S. S. Tyokighir, J. Mom, K. E. Ukhurebor, and G. Igwue, “New developments and trends in 5G technologies: applications and concepts,” *Bulletin of Electrical Engineering and Informatics*, vol. 13, no. 1, pp. 254–263, Feb. 2024, doi: 10.11591/eei.v13i1.6032.

[3] R. R. Elsharkawy, Khalid. F. A. Hussein, and A. E. Farahat, “Dual-Band (28/38 GHz) Compact MIMO Antenna System for Millimeter-Wave Applications,” *Journal of Infrared, Millimeter, and Terahertz Waves*, vol. 44, no. 11–12, pp. 1016–1037, Dec. 2023, doi: 10.1007/s10762-023-00943-0.

[4] J. Xiao, Q. Gan, Z. Ye, C.-Z. Han, T. Ding, and Q. Ye, “A 60-GHz Wideband High-Efficiency Circularly Polarized Dual-Coil Antenna Array,” *Sensors*, vol. 25, no. 7, pp. 1-11, Mar. 2025, doi: 10.3390/s25072211.

[5] T. S. Mneesy, R. K. Hamad, A. I. Zaki, and W. A. E. Ali, “A Novel High Gain Monopole Antenna Array for 60 GHz Millimeter-Wave Communications,” *Applied Sciences*, vol. 10, no. 13, pp. 1-14, Jun. 2020, doi: 10.3390/app10134546.

[6] J. C. M. Quintero, E. P. E. Cuesta, and G. L. E. Quiroga, “Design, Analysis, and Simulation of 60 GHz Millimeter Wave MIMO Microstrip Antennas,” *Journal of Sensor and Actuator Networks*, vol. 11, no. 4, pp. 1-15, Sep. 2022, doi: 10.3390/jsan11040059.

[7] M. S. Rabbani and H. Ghafouri-Shiraz, “Ultra-Wide Patch Antenna Array Design at 60 GHz Band for Remote Vital Sign Monitoring with Doppler Radar Principle,” *Journal of Infrared, Millimeter, and Terahertz Waves*, vol. 38, no. 5, pp. 548–566, May 2017, doi: 10.1007/s10762-016-0344-z.

[8] S. R. Govindarajulu, R. Hokayem, and E. A. Alwan, “A 60 GHz Millimeter-Wave Antenna Array for 3D Antenna-in-Package Applications,” *IEEE Access*, vol. 9, pp. 143307–143314, 2021, doi: 10.1109/ACCESS.2021.3121320.

[9] P. Petroutsos and S. Koulouridis, “A mm-Wave 5G Double Slot Array Antenna Based on Gap Waveguide Technology and Glide Symmetries,” *IEEE Access*, vol. 13, pp. 18152–18163, 2025, doi: 10.1109/ACCESS.2025.3532021.

[10] J. Lee, S. Park, J. Choi, W. Park, and K.-Y. Jung, “Compact series-fed microstrip patch array antenna in the 60 GHz band,” *AEU - International Journal of Electronics and Communications*, vol. 187, Dec. 2024, doi: 10.1016/j.aeue.2024.155513.

[11] R. R. Turjo, S. M. Real, and M. H. Sagor, “Phased Array Antenna with Key Shaped Elements for 60 GHz mmWave Communications,” in *2019 International Workshop on Antenna Technology (iWAT)*, Miami, FL, USA: IEEE, Mar. 2019, pp. 178–181, doi: 10.1109/IWAT.2019.8730642.

[12] A. S. A. Gaid *et al.*, “High-gain miniaturized comb-shaped microstrip antenna for 60 GHz band applications: Design and analysis,” *Results in Optics*, vol. 19, pp. 1-12, May 2025, doi: 10.1016/j.rio.2025.100798.

[13] R. N. Tiwari, D. Sharma, P. Singh, and P. Kumar, “A flexible dual-band 4×4 MIMO antenna for 5G mm-wave 28/38 GHz wearable applications,” *Scientific Reports*, vol. 14, no. 1, pp. 1-15, Jun. 2024, doi: 10.1038/s41598-024-65023-2.

[14] M. F. Ahmed, M. I. Ahmed, A. A. Ibrahim, and S. M. Gaber, “Quad-port 28/38 GHz Antenna with Isolation Improvement for 5G Wireless Networks,” *Journal of Infrared, Millimeter, and Terahertz Waves*, vol. 45, no. 7–8, pp. 672–693, Aug. 2024, doi: 10.1007/s10762-024-00993-y.

[15] B. O. Icmez and C. Kurnaz, “High-Gain Dual-Band Microstrip Antenna for 5G mmWave Applications: Design, Optimization, and Experimental Validation,” *Applied Sciences*, vol. 15, no. 7, pp. 1-24, Apr. 2025, doi: 10.3390/app15073993.

[16] P. S. B. Ghouse *et al.*, “Dual-Band Antenna at 28 and 38 GHz Using Internal Stubs and Slot Perturbations,” *Technologies*, vol. 12, no. 6, pp. 1-23, Jun. 2024, doi: 10.3390/technologies12060084.

[17] A. R. Sabek, A. A. Ibrahim, and W. A. Ali, “Dual-Band Millimeter Wave Microstrip Patch Antenna with StubResonators for 28/38 GHz Applications,” in *6th International Conference on Advanced Technology and Applied Sciences (ICaTAS 2021)*, vol. 2128, no. 1, pp. 1-10, Dec. 2021, doi: 10.1088/1742-6596/2128/1/012006.

[18] M. Hussain *et al.*, “Design and Fabrication of a Printed Tri-Band Antenna for 5G Applications Operating across Ka-, and V-Band Spectrums,” *Electronics*, vol. 10, no. 21, pp. 1-10, Oct. 2021, doi: 10.3390/electronics10212674.

[19] R. Ullah, S. Ullah, S. M. Umar, R. Ullah, and B. Kamal, “Design and Modeling of a 28/38/60/70/80 GHz Antenna for Fifth Generation (5G) Mobile and Millimeter Wave (mmW) Applications,” in *2019 International Conference on Electrical, Communication, and Computer Engineering (ICECCE)*, Swat, Pakistan: IEEE, Jul. 2019, pp. 1–7, doi: 10.1109/ICECCE47252.2019.8940640.

[20] O. Ossa-Molina and F. López-Giraldo, “A Simple Model to Compute the Characteristic Parameters of a Slotted Rectangular Microstrip Patch Antenna,” *Electronics*, vol. 11, no. 1, pp. 1-17, Jan. 2022, doi: 10.3390/electronics11010129.

[21] M. N. Srifi, S. K. Podilchak, M. Essaaidi, and Y. M. M. Antar, “Compact Disc Monopole Antennas for Current and Future Ultrawideband (UWB) Applications,” *IEEE Transactions on Antennas and Propagation*, vol. 59, no. 12, pp. 4470–4480, Dec. 2011, doi: 10.1109/TAP.2011.2165503.

[22] A. Iqbal *et al.*, “Frequency and Pattern Reconfigurable Antenna for Emerging Wireless Communication Systems,” *Electronics*, vol. 8, no. 4, pp. 1-12, Apr. 2019, doi: 10.3390/electronics8040407.

[23] A. Ghaffar *et al.*, “A Flexible and Pattern Reconfigurable Antenna with Small Dimensions and Simple Layout for Wireless Communication Systems Operating over 1.65–2.51 GHz,” *Electronics*, vol. 10, no. 5, pp. 1-13, Mar. 2021, doi: 10.3390/electronics10050601.

[24] Z. Pourgholamhossein and T. A. Denidni, “Frequency Reconfigurable Antenna for 5G Millimeter-Wave Applications,” in *2021 IEEE International Symposium on Antennas and Propagation and USNC-URSI Radio Science Meeting (APS/URSI)*, Singapore, Singapore: IEEE, Dec. 2021, pp. 1057–1058, doi: 10.1109/APS/URSI47566.2021.9703719.

[25] R. Ullah *et al.*, “Wideband and High Gain Array Antenna for 5G Smart Phone Applications Using Frequency Selective Surface,” *IEEE Access*, vol. 10, pp. 86117–86126, 2022, doi: 10.1109/ACCESS.2022.3196687.

[26] M.-M. Li, Z.-X. Guan, H.-L. Peng, Y.-B. Li, W.-H. Li, and J.-F. Mao, “Low Profile High Gain and Compact Planar Antenna Array for 60 GHz Radars,” in *2020 International Conference on Microwave and Millimeter Wave Technology (ICMMT)*, Shanghai, China: IEEE, Sep. 2020, pp. 1–3, doi: 10.1109/ICMMT49418.2020.9386813.

[27] M. El Halaoui, L. Canale, A. Asselman, and G. Zissis, “Dual-Band 28/38 GHz Inverted-F Array Antenna for Fifth Generation Mobile Applications,” in *The 14th International Conference on Interdisciplinarity in Engineering&INTER-ENG 2020*, MDPI, Dec. 2020, pp. 1-9, doi: 10.3390/proceedings2020063053.

BIOGRAPHIES OF AUTHORS

Ahmed El Ghandour is a math's teacher at high school in Casablanca, Morocco. He holds a master's degree in electronics and telecommunications. He is currently a Ph.D. student at Advanced Systems Engineering Laboratory, National School of Applied Sciences (ENSA), Ibn Tofail University in Kenitra, Morocco. His research areas are antennas, mm Wave, 5G applications, metamaterials, reconfigurable array antennas, cognitive radio, and mobile networks. He can be contacted at email: ahmed.elghandour@uit.ac.ma.

Mohamed Nabil Srifi is currently the Director of the National School of Applied Sciences, Ibn Tofail University, Kenitra, Morocco, Full Professor of Electrical Engineering at National School of Applied Sciences ENSAK, Ibn Tofail University, Morocco. He received the bachelor's degree in electrical engineering and Ph.D. in Telecommunication Systems Engineering, respectively, in 1999 from Ibn Tofail University and 2009 from Abdelmalek Essaadi University. His research interests include microwave engineering, antennas design, intelligent RF front ends, computational electromagnetics, biomedical engineering and smart systems. He is the president of Moroccan institute for sciences and development (MISD). He is a member of the IEEE, IEEE communication society, IEEE microwave theory and techniques society, IEEE antennas and propagation society, European microwave association, and the Moroccan association for advanced materials. He holds two patents on antennas for ultra-wide band applications, and he is a recipient of national and international awards. He is the author and coauthor of several papers which appeared in referred international journals and conferences. He serves as reviewer for international journals, e.g., (IEEE Transactions on Industrial Electronics, Elsevier Computers and Electrical Engineering Journal, Wiely Microwave and Optical Technology Letters, Turkish Journal of Electrical Engineering and Computer Sciences, International Journal of Electronics and Communications, International Journal of Microwave, and Optical Technology). He acted as TPC member for international conferences and symposiums. He is the founder and the general chair of the international symposium on advanced electrical and communication technologies (ISAECT). He can be contacted at email: srifimn@gmail.com.

Younes Karfa Bekali is a full Professor of Physics at the Faculty of Sciences of Mohammed V University in Rabat, Morocco. He is a member of the research laboratory in computer science and telecommunications (LRIT) at the same university. Holding a Ph.D. in Physics with a specialization in electronics and telecommunications from the Faculty of Sciences of Tetuan, he is also the Director of the Center for Innovation and Technology Transfer at the Faculty of Sciences of Rabat (CITT-FSR). A prolific inventor and innovator, He is the holder of several patents and has been recognized with numerous national and international awards for his innovative work. Certified as a trainer in industrial property and patents by the Moroccan office of industrial and commercial property (OMPIC), he is also a consultant and expert in these fields. His areas of expertise include electronics and telecommunications engineering, antenna engineering, and intellectual property. He has made significant contributions to the field through numerous publications in international journals and conferences. He can be contacted at email: y.bekali@um5r.ac.ma.

Mourad El Habchi is an accomplished assistant professor in the Faculty of Science Ben M'sick Casablanca, specializing in electronic engineering, telecommunications engineering, and communication engineering. With a wealth of knowledge and expertise in these fields, he has made significant contributions to the academic and research community he has published more than 14 papers. Their research and teaching focus on cutting-edge technologies, with a particular emphasis on antennas. He possesses a deep understanding of antenna design, optimization, and performance evaluation, making them a sought-after expert in this area. He can be contacted at email: mouradelhabchi@hotmail.fr.